Research Article

Computational Fluid Dynamics Simulation of Multiphase Flow in Structured Packings

Saeed Shojaee,[1] Seyyed Hossein Hosseini,[2] and Behzad Saeedi Razavi[3]

[1] *Department of Chemical Engineering, University of Sistan and Baluchestan, Zahedan 98164-161, Iran*
[2] *Department of Chemical Engineering, Faculty of Engineering, Ilam University, Ilam 69315-516, Iran*
[3] *Institute of Standard and Industrial Research of Iran, Khorasan Razavi 9185837733, Iran*

Correspondence should be addressed to Seyyed Hossein Hosseini, s.h.hosseini@mail.ilam.ac.ir

A volume of fluid multiphase flow model was used to investigate the effective area and the created liquid film in the structured packings. The computational results revealed that the gas and liquid flow rates play significant roles in the effective interfacial area of the packing. In particular, the effective area increases as the flow rates of both phases increase. Numerical results were compared with the Brunazzi and SRP models, and a good agreement between them was found. Attention was given to the process of liquid film formation in both two-dimensional (2D) and three-dimensional (3D) models. The current study revealed that computational fluid dynamics (CFD) can be used as an effective tool to provide information on the details of gas and liquid flows in complex packing geometries.

1. Introduction

Corrugated sheet structured packing has been widely used in gas-liquid contacting devices of industrial application for improving performance [1]. Several parameters cause the structured packings to be popular: attaining the minimal pressure drop per theoretical stage while achieving high separation efficiency, allowing reduction in energy dissipation, increasing loading capacity, and increasing the flooding capacity to its higher values [2].

Structured packings are made of corrugating metal or plastic sheets that are arranged side by side with opposing channel orientations. Channels are oriented with the angle of $\pm\beta$ from the horizontal direction. This angle usually varies from 45° to 60°. To create the elements, corrugated sheets are alternately arranged parallel to one another. Structured packing

performance depends on the characteristic of the corrugation geometry. The 45°-corrugation-angle structured packings are prevalent in the gas-liquid separation industry. The 60°-corrugation angle is designed for high capacity processes.

The rate of mass transfer for a structured packed column strongly depends on the effective interfacial area of the bed. In most cases, the effective surface for mass transfer is different from the geometrical surface area of the sheets due to the effects of hydraulic conditions and physical interactions that influence the spreading of liquid on the sheets.

A number of theoretical, semiempirical, and empirical correlations for predicting the effective interfacial area in structured packings have been reported in the literature. These models are developed for different packings and various process conditions using physical measurement methods such as electroresistivity and light transmission. Only a few researchers have reported actual interfacial areas for limited kinds of structured packings [3]. Most of the distillation data used in the correlations reported in the literature have been extracted under total reflux conditions. Thus, the liquid and gas velocities effects could not be studied separately from the available data. In some reported models, there is no explicit effect of the gas velocity, and only the liquid phase effects are considered to include the effect of surface wetting. Only a very few works consider the consequence of gas loading [4, 5]. Some researchers have suggested that the interfacial area can be larger than the packing geometry area; however, there are some disagreements on this issue. A brief review of the parameters that influence the interfacial area has been presented in the previous work [6].

The wetting process of the packing surface is quite complex and is not fully understood. In the recent years, computational fluid dynamics (CFD) has become a useful tool for analyzing multiphase flows in various industrial applications. In particular, CFD provides the capability to reduce a number of required experiments for describing the flow pattern inside complex geometries such as structured packings; as a result, it reduces the cost of design for the required equipment.

There have been a number of computer modeling flows in structured packings. For simulating the hydrodynamics of liquid phase flow in structured packing filled with catalyst pellets, Van Gulijk [7] used the Toblerone model, simplified the multiphase flow for a single phase in the channels, and evaluated the transversal dispersion in the structured packed bed. Van Baten et al. [8, 9] investigated the liquid dispersion and gas and liquid phase mass transfer between two sheets of KATAPAK-S structured packing using CFD tool. They considered mass transfer of the gas phase in an empty channel, as well as liquid phase mass transfer within the catalyst-packed channels. Petre et al. [10] and Larachi et al. [11] proposed the structured packing as a combination of four representative elementary 3D units (REU) and evaluated the dry pressure drop of the bed. Szulczewska et al. [12] employed a 2D model, and assumed countercurrent gas-liquid flows, to investigate the mechanisms of droplet formation and liquid film breakup over both flat and corrugated vertical plates. They evaluated the gas-liquid interfacial area using film thickness in a 2D model. Based on Petre and Larachi's work [10, 11], Raynal et al. [13] predicted the dry pressure drop of structured packing. They estimated the thickness of the liquid film and consequently the liquid hold-up in a structured packing under cocurrent flow using the VOF approach. Ataki and Bart [14] applied the flat packing element of Rombopak 4 M in their CFD models and described the degree of wetting and the effective area. They also investigated the effect of liquid properties on the degree of wetting. Haghshenas Fard et al. [15] presented a CFD model to predict both dry and wet pressure drops for the entire packing module. They also determined the mass transfer efficiency of the packing in two packing sheets. Mahr and Mewes [16] proposed a model for two-phase flows in columns with structured packing. They calculated the pressure

drop in the packing at different angles and directions. Using this model, the macroscopic flow field of countercurrent two-phase flow could be evaluated in strong anisotropic porous structures. Khosravi Nikou and Ehsani [17] implemented different turbulence models to study the flow through structured packings and investigated heat and mass transfers in the packing. Fernandes et al. [18, 19] assumed uniform wetting of the packing surface and presented a pseudo single-phase CFD model for determination of wet pressure drops of a Sulze BX packing element in supercritical fluid extraction process.

In summary, a few studies have been reported in the existing literature that use CFD techniques for evaluating the effective areas in structured packings while most of the studies are restricted to prediction of the pressure drop and the use of 2D models for the two-phase flow simulations. In addition, liquid film thickness in 2D and 3D frameworks was investigated rarely in the past. In this study, a 3D computational framework was used by considering multiphase flow for the domain within two layers of the largest element of the structured packings. The evaluation of the effective area was based on the liquid film thickness using the VOF method in the 3D simulation. Countercurrent motions of air and water as gas and liquid phases, respectively, were analyzed, and the effective areas, liquid hold-up, liquid and gas velocities as well as liquid film thickness were evaluated. 2D model was evaluated to study liquid film thickness besides the 3D computational domain.

2. Numerical Simulations

2.1. Governing Equations

The simulations are carried out using the volume of fluid (VOF) model. The VOF approach is well suited for tracking the interface between the two immiscible phases, namely, the gas-liquid interface. VOF solves a single set of momentum equations throughout the domain, while keeping track of the volume of phases in each computational cell. The resulting velocity in each cell is the mass averaged values of the phases present in the cell. The corresponding momentum balance equation for the two-phase flow is given as

$$\frac{\partial}{\partial t}(\rho\vec{v}) + \nabla \cdot (\rho\vec{v}\vec{v}) = -\nabla \cdot P + \nabla \cdot \left[\mu\left(\nabla\vec{v} + \vec{v}^T\right) \right] + \rho\vec{g} + \vec{F}, \qquad (2.1)$$

where ρ is the fluid density and $\vec{v}$ the velocity vector. In addition, P, $\rho\vec{g}$, and $\vec{F}$ are the static pressure, the gravitational body force, and the external body forces, respectively. Equation (2.1) involves the volume fractions of both phases that enter through the physical properties of the phases such as density and viscosity. Accordingly, the phase-averaged properties are given as

$$\rho = \alpha_1\rho_1 + \alpha_2\rho_2,$$
$$\mu = \alpha_1\mu_1 + \alpha_2\mu_2, \qquad (2.2)$$

where ρ and α are density and volume fractions and the subscripts correspond to the phases. In each control volume, summation of all the phase volume fractions is equal to unity. That is,

$$\sum_{i=1}^{n} \alpha_i = 1. \qquad (2.3)$$

The tracking of the interface is done in the cells where the volume fraction is different from 0 or 1. If a cell is completely filled with one phase, the volume fractional of that phase in the cell is equal to unity ($\alpha = 1$), and the cell is considered to be in the main flow region of that phase. A cell is considered to be on the (interface) free surface when the value of volume fraction is between 0 and 1 ($0 < \alpha < 1$). The tracking of the interface(s) between the phases is accomplished by the solution of a continuity equation for the volume fraction of one (or more) of the phases. For the ith phase this equation is written as

$$\frac{\partial}{\partial t}(\alpha_i \rho_i) + \nabla \cdot (\alpha_i \rho_i \vec{v}_i) = 0. \tag{2.4}$$

In the present study, mass transfer terms between the immiscible water and air phases are neglected [18, 19]. The VOF model, however, accounts for the effect of surface tension along the interface between the phases. The surface tension model used in these simulations is the continuum surface force (CSF) model that was proposed by Brackbill [20]. The CSF model can be augmented by the additional prescription of the contact angles between the phases and the walls. The wall may absorb the liquid (wetting wall) or repel the liquid (nonwetting wall), and the contact angle varies depending on the hydrophobicity of the wall. The equilibrium contact angle depends also on the smoothness of the wall [20].

One important part of a CFD simulation is the use of an appropriate turbulence model. In the present study, based on previous work [21] and the CFD model of Khosravi Nikou and Ehsani [17] for simulation of a structured packing, the BSL model (the baseline k-ω model) is used for the present simulations. The main problem with the k-ω model is its well-known strong sensitivity to free stream conditions. This is undesirable, and, in order to solve the problem, the BSL model that is a blending between the k-ω model near the surface and the k-ε model in the outer region is developed.

Typically, the relative error between two successive iterations is specified using a convergence criterion of 10^{-4} for each scaled residual component. It might be worth mentioning the computational time required for each 3D simulation run, which is about 6-7 days while this time duration is about 20–25 hours for each 2D simulation run on a Pentium 4 CPU running on a quad-core 3.2 GHz with 4 GB of RAM.

For the current simulations, the phases are air and water. The fluids are assumed to be Newtonian, isothermal, and incompressible; therefore, their properties are kept constant. The computations are conducted under the unsteady state condition, with a time step of 0.002 sec until a pseudosteady state is reached. Pseudosteady conditions are established when the mass flow rates at the outlets do not change. The physical properties of the phases and the geometrical characteristics used in the simulations are listed in Tables 1 and 2.

2.2. Domain and Grid Arrangements

To investigate the effective area, the experimental setup of Rocha et al. [22] is utilized for validation and verification of the 3D CFD model. The computational space for the CFD model consists of 34 triangular channels, with a total number of 137 crossovers, which is shown in Figure 1. Since the thickness of the liquid film on the packing surface is very small, a refined structural grid is used for achieving better convergence and for decreasing the number of grid elements in the domain. The grids are dense near the wall for more accurate determination of the liquid film thickness, and they become coarser away from the wall.

Table 1: Physical properties of the system for simulations.

Physical properties	Air	Water
Density ρ (kg m^{-3})	1.185	997
Kinematic viscosity υ (m^2 s^{-1})	1.545 10^{-5}	8.926 10^{-7}
Surface tension σ (N m^{-1})	—	0.0728
Static contact angle with air steel	—	70–80°

Table 2: Geometrical characteristics for the simulated structured packing.

Packing type	Sulzer BX	Gempak 2A
Specific surface area (m^2/m^3)	500	223
Height of element (m)	0.185	0.2477
Void fraction (%)	90	95
θ (deg)	55	45
a_p (m^{-1})	—	223
Channel dimensions (m)		
Height of triangle (h)	0.006	0.0122
Base of triangle (b)	0.012	0.0267
Corrugation spacing (s)	0.009	0.018

Grid independence of the solution was tested through using several different grid sizes. Table 3 shows the predicted liquid film thickness using various mesh sizes. This table shows that when finer grids are used the predicted liquid film thickness is reduced. Against the coarse grids, the predicted liquid film thicknesses for both fine and medium grids are roughly close. The simulation running time on the fine grid takes considerable CPU time. Consequently, simulations are conducted on the medium grid with a total number of computational hexahedral cells of 1315200, 22100, and 17280 for 3D and 2D frameworks of Gempak 2A as well as 2D modeling of Sulzer BX, respectively.

To investigate liquid film formation on the packing in a 2D computational framework, the experimental setups of Rocha et al. [22] and Cho et al. [23] at Gempak 2A and Sulzer BX packings, respectively, are used. In a 2D domain, a cross-section of the packing channel is obtained when the duct between two corrugated plates is cut vertically.

2.3. Initial and Boundary Conditions

For the 3D model (Rocha et al. [22] setup) on the lower side of the packing sheets, the uniform inlet velocity boundary conditions are prescribed for both air and water phases. In this section of the packing, the velocity inlets are identified where gas and liquid velocities in that region have, respectively, positive and negative values to hold countercurrent flows in the simulation process. The outlet is defined on the upper side of the packing sheets using the pressure outlet boundary condition. At this boundary, the outlet static pressure is prescribed. A no-slip boundary condition is used for the gas and liquid phases on the lateral walls of the packing. The computational domain is assumed to be initially filled with air, and the initial volume fraction of the water is set to zero. In addition, the initial values of gas and liquid velocities are set to zero through the packing element.
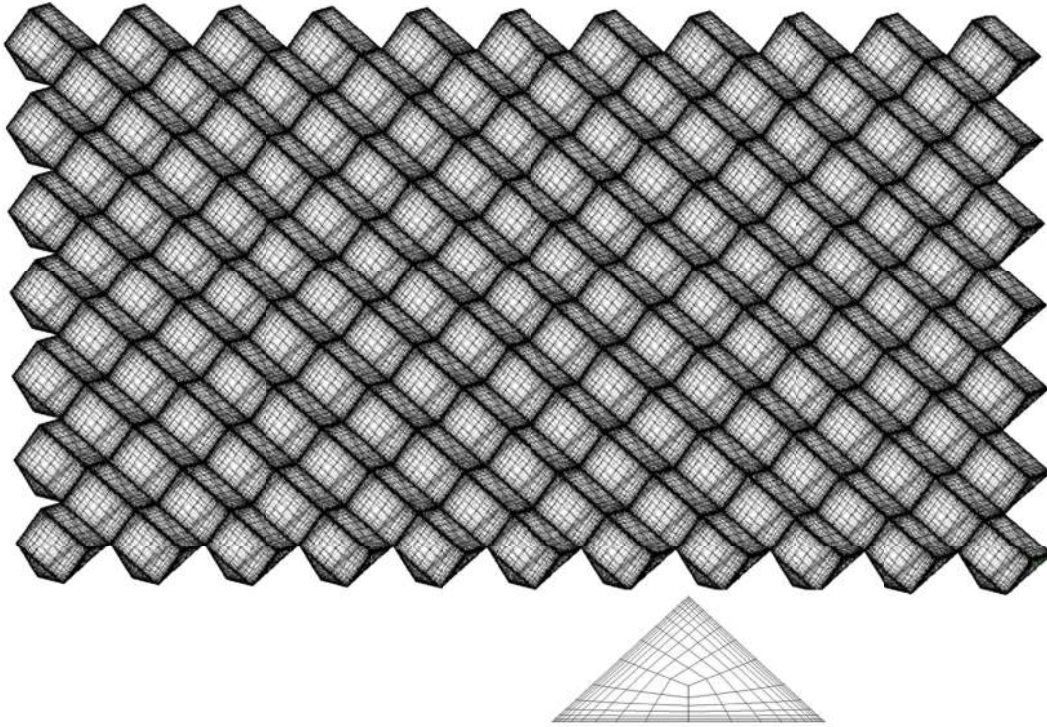
Figure 1: Computational domain for simulation and schematic overview of meshing of a triangular face.

Table 3: Liquid film thickness at different mesh sizes.

	Fine	Medium	Coarse
Rocha et al. [22] (for 3D modeling)			
Number of computational cells	1657700	1315200	771584
Liquid film thickness (mm)	0.26	0.269	0.372
Rocha et al. [22] (for 2D modeling)			
Number of computational cells	25000	22100	15500
Liquid film thickness (mm)	0.275	0.28	0.31
Cho et al. [23] (for 2D modeling)			
Number of computational cells	20000	17280	10500
Liquid film thickness (mm)	0.265	0.27	0.30

For the 2D two-phase flow simulations (Rocha et al. [22] and Cho et al. [23]), the liquid and gas inlet zones are defined with uniform inlet velocity boundary conditions. The outlets for liquid and gas are defined with an outflow boundary condition. The computational domain is assumed to be initially filled with air, and the initial volume fraction of the water is set to zero. At the walls, a no-slip boundary condition for gas and liquid phases is imposed according to the previous works. The static contact angle of $\gamma = 70°$ is also assumed.

3. Results and Discussion

3.1. Pressure Drop

Pressure drop is an important measured parameter that can be used to validate hydrodynamic models of multiphase systems. Here the predicted pressure drops are compared with the experimental data. A commonly used model for determining mass transfer and pressure drop in structured packings was developed several years ago at the separations research program (SRP) of the University of Texas at Austin. Rocha et al. [22] treated structured packing as a network of wetted wall columns and theorized that the effective area, pressure drop, and hold-up should be all related. They proposed following correlation for dry pressure drop of the packings,

$$\frac{\Delta P_{\mathrm{dry}}}{Z} = \frac{0.177\rho_G}{S\varepsilon^2(\sin\theta)^2}U_{gS}^2 + \frac{88.774\mu_G}{S^2\varepsilon\sin\theta}, \tag{3.1}$$

where U_{gS} and ε, respectively, are superficial gas velocity and void fraction of packing and S stands for side dimension of corrugation.

The irrigated pressure drop was also proposed by Rocha et al. [22], based on a generic channel model, as

$$\frac{\Delta P_{\mathrm{dry}}}{Z} - \frac{\Delta P}{Z}[1 - (0.614 + 71.35S)h_L]^5 = 0. \tag{3.2}$$

The CFD results are compared with the corresponding experimental data and SRP model results. Figure 2 shows the predicted dry pressure drops of CFD tool and SRP model against the F-factor, $u_G(\rho_G)^{0.5}$, in the structured packing. The experimental data of Rocha et al. [22] are reproduced in this figure to compare with the CFD results and SRP model predictions. The mean absolute relative error of the CFD dry pressure drop is about 13.4%. A major reason for the under-prediction of the pressure drop in Figure 2 is that the junction effect between two consecutive packing layers is not considered in the simulations. More details regarding this effect are found in Petre et al.'s [10] work. Therefore, under-prediction of the pressure drop results of the present model is anticipated. However, the SRP model slightly overpredicts the pressure drop in comparison with the experimental data.

Figure 3 depicts the predicted irrigated pressure drops of CFD tool and SRP model against the F-factor in the structured packing. The experimental data of Rocha et al. [22] are again reproduced in this figure to compare with SRP model predictions and CFD results. As can be seen in this figure, the SRP model overestimates the wet pressure drop in the F-factor higher than $3.5\,\mathrm{m/s(kg/m^3)^{0.5}}$ and predicts the best results in lower range of the F-factor. However, the CFD results show the same trend with the experimental data especially in higher F-factors. By reaching the flooding region, CFD predicts the better results in comparison with the SRP model. Generally, pressure drop in two-phase flow containing gas-liquid interaction is increasing due to the change in flow direction and gas-gas interactions. Therefore, the model predicts acceptable results in terms of dry and irrigated pressure drops. Consequently, the current model can be used to examine the behavior of the other hydrodynamic parameters in the structured packings.
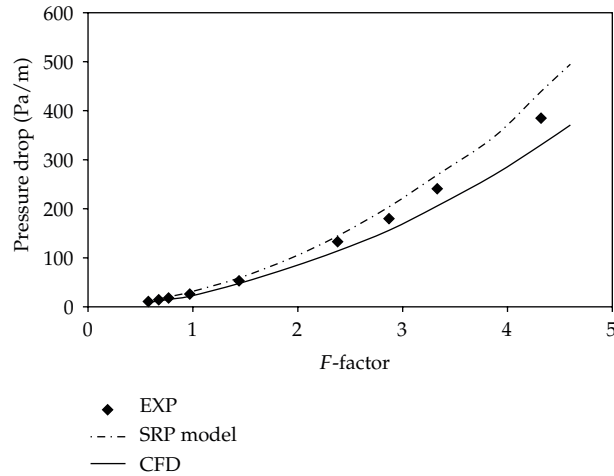
Figure 2: Comparison between predicted dry pressure drops of CFD tool and SRP model and experimental data [22] for different F-factors in the structured packing.
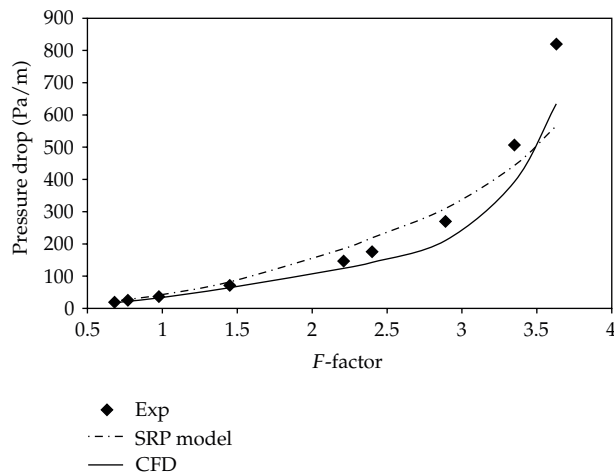

Figure 3: Comparison between predicted wet pressure drops of CFD tool and SRP model and experimental data [22] for different F-factors in the structured packing.

3.2. Effective Area

The effective area for mass transfer is defined as the absolute effective area divided by the packing volume (m^2/m^3). Knowledge of the value of this parameter and the effective factors upon it can be useful for the design of packings in separation columns. In this study, the effective area is evaluated from the values of liquid hold-up per estimated liquid film thickness based on the earlier work of Iliuta and Larachi [24]:
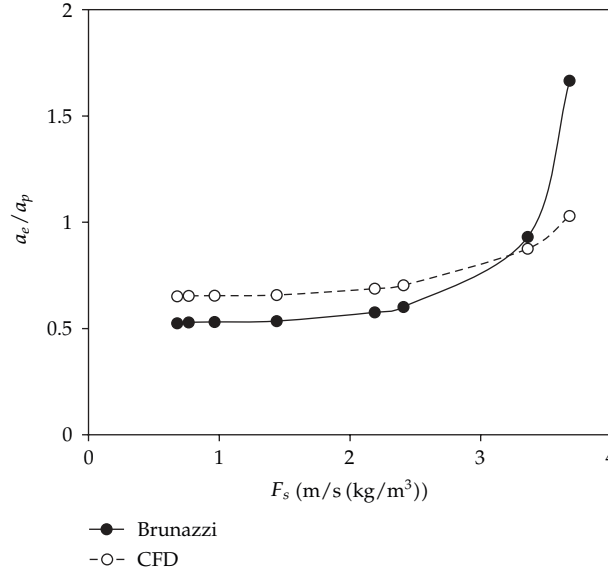
$$a_e = \frac{h_L}{\delta_{\text{CFD}}},\tag{3.3}$$

Figure 4: Comparison between the CFD results and the Brunazzi model by increasing gas velocity.

where a_e and δ_{CFD} represent the effective area of packing and average liquid film thickness. Simulations are carried out for a water superficial velocity of $0.007\,\text{m/s}$ and different gas capacity factors ($F_s = u_G \sqrt{\rho_G}$). Based on the evaluated average thickness of the rivulets, the surface area of liquid rivulets is determined.

Figure 4 compares the CFD results for the ratio of the predicted effective interfacial area to the packing surface area (a_e/a_p) with the Brunazzi et al. [25] correlation. The use of the correlation suggested by Brunazzi et al. [25] requires only a simple experimental estimate of the liquid hold-up. The correlation is as follows:

$$\frac{a_e}{a_p} = \frac{d_{\text{eq}}}{4}\left(\frac{h_L}{\varepsilon}\right)^{1.5}\left[\frac{\rho_L g \varepsilon (\sin\theta)^2}{3\mu_L u_L}\right]^{0.5}. \tag{3.4}$$

The simulation results show that, in the preloading zone, the effective area is a weak function of the gas flow rate. This is due to the weak interactions between gas and liquid phases. It is observed that with increasing the superficial gas velocity, the effective area of the packing is increasing, resulting in the corresponding mass transfer rate increase. At gas flow factor of $3.68\,\text{m/s}\,(\text{kg/m}^3)$, the effective area is equal to the packing surface area. On the other hand, a higher gas rate increases the instability in liquid flow and leads to a higher effective interfacial area. The Brunazzi et al. [25] correlation predicts the rise of effective area and shows a good agreement with the CFD results. As can be seen in Figure 4, at the capacity higher than 3.25, the Brunazzi et al. [25] correlation overpredicts the effective area in comparison with the CFD results. It is also seen that the slope of the calculated curve by the Brunazzi et al. [25] correlation increases suddenly because experimental hold-up in this correlation reflects indirectly the gas velocity effect.

As it is shown in Figure 4, the computed fractional area, a_e/a_p, is approximately constant in the range of gas velocity (F_s) from 2.4 to $680\,\text{m/s}\,(\text{kg/m}^3)$ but it increases with
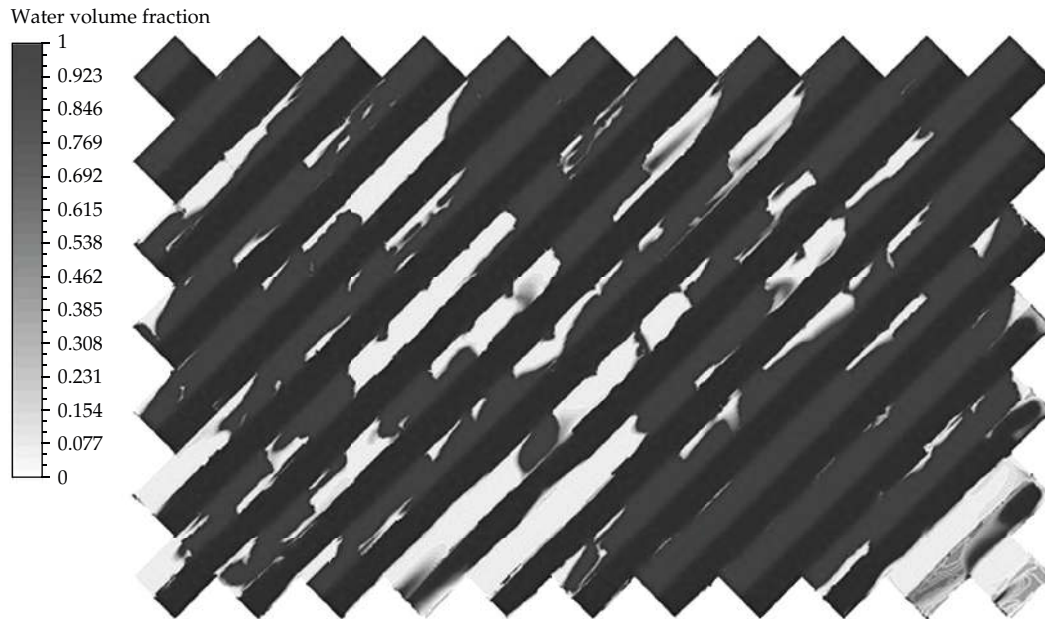
Water volume fraction

Figure 5: Typical liquid flow on surface of corrugation sheet.

increasing the gas velocity ($F_s > 2.41 \, \mathrm{m/s} \, (\mathrm{kg/m^3})$). It is therefore concluded that, in addition to the liquid flow rate, the structured packing interfacial areas are moderately influenced by the gas flow rate.

The distribution of liquid on the surface of packing is a complex phenomenon. Figure 5 illustrates the liquid distribution on the corrugation sheet area. The presence of both dry and wet patches on the packing surface is clearly seen from this figure. This figure shows that liquid not only flows in the channel in which it has been supplied but also flows into the other channels. That is, the liquid is mixed with adjacent streams and the packing surface is covered by a thin liquid layer.

In this step, the laminar flow condition with the assumption that the gas phase does not flow in the packings is made. Thus, the gas phase is considered stagnant with zero velocity and does not affect the liquid flow. This assumption may be a reasonable starting approximation due to the fact that the gas flow has small effect on the liquid flow in the packing.

The efficiency of the packed columns strongly depends on the flow behavior of the liquid inside the packing. Figure 6 indicates a comparison between the CFD results with the Brunazzi et al. [25] correlation against the liquid load. This figure shows that, by increasing the liquid load, the effective area increases for the Brunazzi et al. [25] correlation as well as for the simulation results. When the entire surface area is covered by the liquid film, the effective area (a_e) remains roughly unchanged. For the area ratio, both the CFD results and the Brunazzi et al. [25] correlation lead to values that do not exceed one.

The possibility of a_e/a_p ratios in excess of unity is not explicitly discussed in the literature. It should be noted here that a_e/a_p ratios higher than one are possible in various gas-liquid mixing devices. An example is the spray towers, where this ratio becomes very
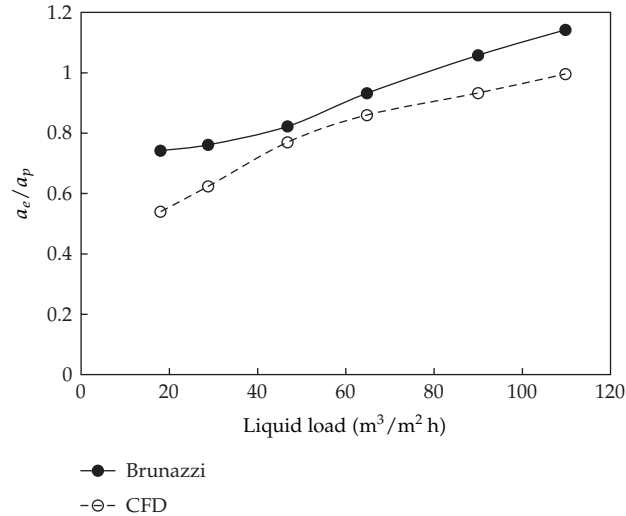
Figure 6: Comparison between the CFD results and the Brunazzi model by increasing the liquid load.

large [26]. Recently, several researchers have estimated the effective interfacial area of structured packings, a_e/a_p, with ratios higher than unity for the flooding regime [26, 27].

The Brunazzi et al. [25] model predicts an increase in the effective area by increasing the liquid loading. It can be seen that the model is in a good agreement with the CFD results especially in the intermediate range of liquid loadings.

Since the gas velocity is assumed zero, the liquid phase forms a film flow downward on the packing surface. Thus, the effective area becomes equal to the packing surface area. The results of the simulations shown in Figure 6 also show that at the flow rate of 109.8 m^3/m^{2}h, when $a_e = a_p$, the total packing surface is covered by water completely.

As an important result, the Brunazzi et al. [25] model, which has been derived based on several parameters, such as liquid hold-up value, geometric parameters, and physical properties of gas and liquid phases, predicts the interfacial area accurately without introducing any adjustable parameter. As noted before, it can be emphasized that the Brunazzi et al. [25] model is independent from the packing type.

Several researchers have studied the effective interfacial area for the different structured packings by experiments and using some published empirical models [28–30]. They have found a similar trend (qualitative agreement) with the results of this study (Figures 4 and 6) and different values of this term quantitatively. The difference in performance of various packings may be attributed to undesirable liquid pooling and bridging for the packings.

3.3. Liquid Flow Pattern

To verify the liquid flow pattern through the structured packing using CFD analysis, X-ray projection of the experimental work of Mahr and Mewes [16] is used for a simple comparison. In the Mahr and Mewes [16] study, the holes in the packing have been sealed in order to keep the liquid between both sheets. Predicted results by the CFD model for the liquid phase behavior confirm the Mahr and Mewes [16] findings. They did not consider gas flow in their measurements similarly to the current study. They found that the liquid film is created in
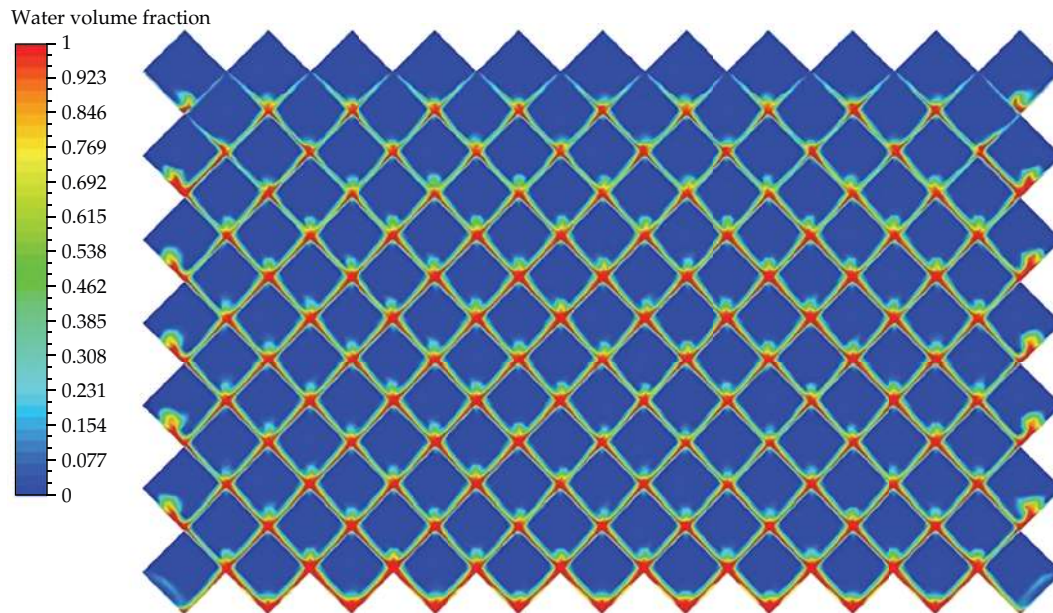
Water volume fraction

Figure 7: Computed liquid film flow on plane between two sheets of Gempak 2A structured packing using CFD.

both inner sides of the packing surface. Their finding is consistent with the current numerical results (Figure 7). Mahr and Mewes [16] observed that at a low liquid flow rate the majority of the liquid is conducted mainly along the flow path with an angle of ±19° with respect to the axial direction. Only a small amount of liquid is kept in the grooves of the corrugation due to surface tension, and the bulk of the liquid phase flows along the corrugation angle of ±42° toward both sides. A local minimum value of liquid hold-up is found straight below the injection point. The experimental results also show that the liquid phase spreads more toward the sides compared to the straight downward flow from the injection point.

Figure 7 shows the predicted liquid film flow on a plane throughout a packing element of Gempak 2A structured packing. The liquid, which flows down the side length of the corrugated sheet channels, mixes and redistributes at the contact points of two sheets. At the mixing point, the film thickness increases and decreases roughly periodically, due to the abrupt change in liquid flow direction and mixing liquid with adjacent streams. In addition, the distribution of liquid in Figure 7 and that in Mahr and Mewes [16] are symmetric with respect to the axial direction at the injection points.

3.4. Liquid Film Thickness

Two sets of 2D simulations for two-phase flows are performed. For the first case, the experimental condition of Cho et al. [23] for Sulzer BX packing is evaluated by the model. Computed size distribution of liquid film thickness along the Sulzer BX packing surface is shown in Figure 8 for a liquid velocity of 0.0101 m/s and F-factor of 0.8 m/s $(\text{kg/m}^3)^{0.5}$. It can be seen from the figure that the liquid film thickness is not uniform. Through a comparison between the Nusselt film thickness, which has been obtained based on the uniform liquid film thickness, and the averaged computed film thickness in the region lower than the loading,
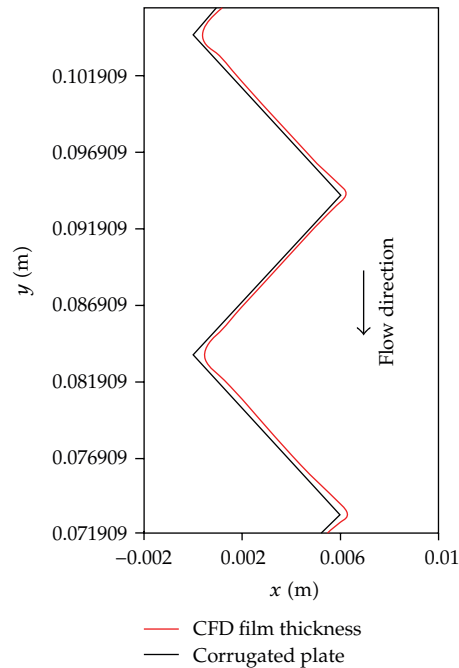
Figure 8: Predicted liquid film thickness along the packing for Sulzer BX at a liquid velocity of $0.0101\,\mathrm{m/s}$ and F-factor of $0.8\,\mathrm{m/s\,(kg/m^3)^{0.5}}$.

it is found that the deviation is about 35%. The average computed liquid film thickness is $0.00027\,\mathrm{m}$.

For the second set of study, the experimental condition of Rocha et al. [22] for Gempak 2A packing is simulated. The computed liquid volume fraction counters in the 2D model of Gempak 2A and Sulzer BX are shown in Figure 9. Here the liquid velocity and F-factor are, respectively, $0.007\,\mathrm{m/s}$ and $2.2\,\mathrm{m/s\,(kg/m^3)^{0.5}}$. From this figure the presence of liquid films on the packing surfaces can be clearly seen, which vary in thickness. Nonuniformity of the film thickness can also be observed in the 3D model results (Figure 7). Figure 9, however, shows that the liquid film thickness in the Gempak 2A packing is more uniform compared to the Sulzer BX. It is also seen that the liquid film is thicker at the intersection of the plates and decreases with distance. Moreover, the liquid film thickness in Gempak 2A packing is thinner than that in Sulzer BX. That is particularly the case at the cornets. When the dimensions of the packing become larger, Gempak 2A, liquid thickness decreases for a constant liquid load due to covering wide surface of the packing by the liquid phase. This behavior is logical; as a result the dimensions of the packing can influence the liquid film thickness.

4. Conclusions

The CFD model for countercurrent two-phase flows in a structured packing was validated by comparison with the experimental data and well-known empirical models of Brunazzi et al. [25] and SRP [22]. The CFD model described the influences of hydrodynamics parameters such as gas velocity and liquid load on the effective mass transfer area. The simulation results indicated that the gas flow rate is an important factor for the mass transfer performance.
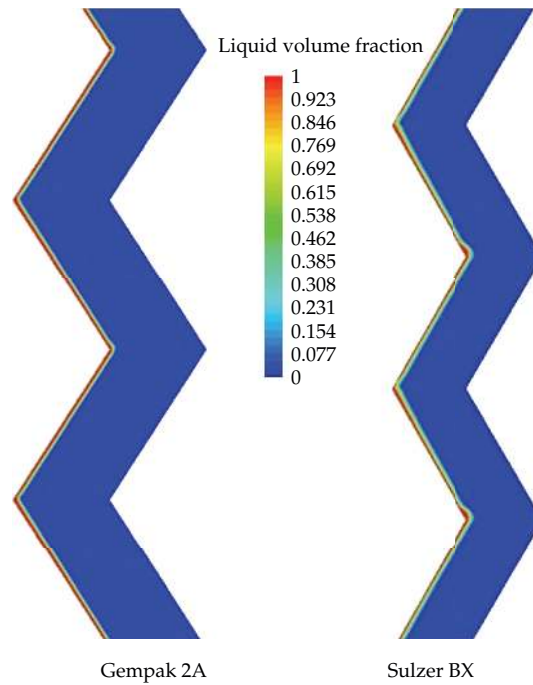
Figure 9: Contours of liquid volume fraction for 2D modeling of Gempak 2A and Sulzer BX (U_L = 0.007 m/s; F-factor = 2.2 m/s $(kg/m^3)^{0.5}$.

Increasing kinetic energy of gas flow to increase the liquid hold-up generates instabilities in liquid film, formation of surface ripples, and creation of droplets that result in higher interfacial area and thus increases the efficiency. An increase of the liquid wetting caused an increase in the packing surface until the liquid covered the entire surface. Beyond that, the rate of increase is small. In addition, the simulations showed that the CFD model is capable for determining the minimum flow rates for an entire surface of structured packing covered with the liquid. CFD tool emphasized the general applicability of the Brunazzi et al. [25] model for the various types of structured packings at different gas and liquid flow rates.

Studying the liquid film flow over the packing surfaces by CFD simulation can lead to a better understanding of the role of the effective parameters on the gas-liquid mass transfer. The process of liquid film formation on the packing surface was studied in details and the parameters that influence the liquid film thickness were discussed. It was shown that, inside the two sheets of structured packing, the maximum thickness of the liquid film was near the contact points of the sheets where liquid was redistributed over the corrugated surface. Such behaviour was observed in both 2D and 3D modelings. CFD showed that the dimensions of the packing could influence the liquid film thickness. In addition, considering uniform liquid film thickness, Nusselt assumption on the structured packings is unacceptable. This matter was observed in both 2D and 3D modelings.

Nomenclature

A: Packing type and size-dependent constants
a_e: Effective mass transfer area, m^2/m^3

a_L: Effective liquid flow angle
a_p: Specific area of packing, m^2/m^3
b: Corrugation base dimension, m
B: The packing type and size-dependent constants
d_{eq}: Equivalent diameter of flow channel
d_h: Hydraulic diameter of packing defined by $4\varepsilon/a_p$
$\vec{F}$:   Additional forces in the Navier-Stokes equations, N
F_s: Gas capacity factor, $u_G(\rho_G)^{0.5}$, $m/s(kg/m^3)^{0.5}$
g: Gravitational acceleration, m/s^2
h: Corrugation crimp height, m
h_L: Liquid hold-up, —
P: Pressure
S: Corrugation side length, m
t: Time, s
u: Velocity, m/s
U_{gS}: Superficial gas velocity, m/s
$\vec{v}$:   velocity vector
Z: Packed height, m.

Dimensionless Numbers

$Fr = u^2/gd_h$:   Froude number

$Re = ud_h/v$:   Reynolds number

$We = u^2\rho d_h/\sigma$: Weber number

Greek Letters

α: Volume fraction, —
γ: Static contact angle, degree
δ: Liquid film thickness, mm
ε: Void fraction of packing, —
θ: Corrugation angle (with respect to the horizontal), degree
μ: Viscosity, Pa .s
v_L: Liquid kinematic viscosity, m^2/s
ρ_L: Liquid density, kg/m^3
σ: Surface tension, N/m
Ω: Packing surface void fraction.

Subscripts

G: Gas phase
i: Index
L: Liquid phase
n: Number of phases.

References

[1] Z. Olujic, M. Behrens, L. Colli, and A. Paglianti, "Predicting the efficiency of corrugated sheet structured packings with large specific surface area," *Chemical and Biochemical Engineering Quarterly*, vol. 18, no. 2, pp. 89–96, 2004.

[2] E. Brunazzi, A. Paglianti, and L. Petarca, "Design of absorption columns equipped with structured packings," *Chimica & Industria*, vol. 78, pp. 459–467, 1996.

[3] S. Shetty and R. L. Cerro, "Fundamental liquid flow correlations for the computation of design parameters for ordered packings," *Industrial and Engineering Chemistry Research*, vol. 36, no. 3, pp. 771–783, 1997.

[4] R. H. Weiland, K. R. Ahlgren, and M. Evans, "Mass-transfer characteristics of some structured packings," *Industrial and Engineering Chemistry Research*, vol. 32, no. 7, pp. 1411–1418, 1993.

[5] Z. P. Xu, A. Afacan, and K. T. Chuang, "Predicting mass transfer in packed columns containing structured packings," *Chemical Engineering Research and Design*, vol. 78, no. 1, pp. 91–98, 2000.

[6] S. Shojaee, S. H. Hosseini, A. Rafati Saleh, and G. Ahmadi, "Prediction of effective area in structured packings by CFD," *Industrial & Engineering Chemistry Research*, vol. 50, pp. 10833–10842, 2011.

[7] C. Van Gulijk, "Using computational fluid dynamics to calculate transversal dispersion in a structured packed bed," *Computers and Chemical Engineering*, vol. 22, no. 1, pp. S767–S770, 1998.

[8] J. M. Van Baten, J. Ellenberger, and R. Krishna, "Radial and axial dispersion of the liquid phase within a KATAPAK-S(R) structure: experiments vs. CFD simulations," *Chemical Engineering Science*, vol. 56, no. 3, pp. 813–821, 2001.

[9] J. M. van Baten and R. Krishna, "Gas and liquid phase mass transfer within KATAPAK-S structures studied using CFD simulations," *Chemical Engineering Science*, vol. 57, no. 9, pp. 1531–1536, 2002.

[10] C. F. Petre, F. Larachi, I. Iliuta, and B. P. A. Grandjean, "Pressure drop through structured packings: breakdown into the contributing mechanisms by CFD modeling," *Chemical Engineering Science*, vol. 58, no. 1, pp. 163–177, 2003.

[11] F. Larachi, C. F. Petre, I. Iliuta, and B. Grandjean, "Tailoring the pressure drop of structured packings through CFD simulations," *Chemical Engineering and Processing*, vol. 42, no. 7, pp. 535–541, 2003.

[12] B. Szulczewska, I. Zbicinski, and A. Górak, "Liquid flow on structured packing: CFD simulation and experimental study," *Chemical Engineering and Technology*, vol. 26, no. 5, pp. 580–584, 2003.

[13] L. Raynal, C. Boyer, and J. P. Ballaguet, "Liquid holdup and pressure drop determination in structured packing with CFD simulations," *Canadian Journal of Chemical Engineering*, vol. 82, no. 5, pp. 871–879, 2004.

[14] A. Ataki and H. J. Bart, "Experimental and CFD simulation study for the wetting of a structured packing element with liquids," *Chemical Engineering and Technology*, vol. 29, no. 3, pp. 336–347, 2006.

[15] M. Haghshenas Fard, M. Zivdar, R. Rahimi et al., "CFD simulation of mass transfer efficiency and pressure drop in a structured packed distillation column," *Chemical Engineering and Technology*, vol. 30, no. 7, pp. 854–861, 2007.

[16] B. Mahr and D. Mewes, "Two-phase flow in structured packings: modeling and calculation on a macroscopic scale," *AIChE Journal*, vol. 54, no. 3, pp. 614–626, 2008.

[17] M. R. Khosravi Nikou and M. R. Ehsani, "Turbulence models application on CFD simulation of hydrodynamics, heat and mass transfer in a structured packing," *International Communications in Heat and Mass Transfer*, vol. 35, no. 9, pp. 1211–1219, 2008.

[18] J. Fernandes, P. C. Simões, J. P. B. Mota, and E. Saatdjian, "Application of CFD in the study of supercritical fluid extraction with structured packing: dry pressure drop calculations," *Journal of Supercritical Fluids*, vol. 47, no. 1, pp. 17–24, 2008.

[19] J. Fernandes, P. F. Lisboa, P. C. Simões, J. P. B. Mota, and E. Saatdjian, "Application of CFD in the study of supercritical fluid extraction with structured packing: wet pressure drop calculations," *Journal of Supercritical Fluids*, vol. 50, no. 1, pp. 61–68, 2009.

[20] J. U. Brackbill, "A continuum method for modeling surface tension," *Journal of Computational Physics*, vol. 100, no. 2, pp. 335–354, 1992.

[21] A. Rafati Saleh, S. H. Hosseini, S. Shojaee, and G. Ahmadi, "CFD studies of pressure drop and increasing capacity in mellapakplus 752.Y structured packing," *Chemical Engineering & Technology*, vol. 34, pp. 1402–1412, 2011.

[22] J. A. Rocha, J. L. Bravo, and J. R. Fair, "Distillation columns containing structured packings: a comprehensive model for their performance. 1. Hydraulic models," *Industrial and Engineering Chemistry Research*, vol. 32, no. 4, pp. 641–651, 1993.

[23] S. Y. Cho, Y. Y. Lee, and S. J. Kim, "A study on characteristics of a modern structured packing," *Korean Journal of Chemical Engineering*, vol. 12, no. 3, pp. 313–319, 1995.

[24] I. Iliuta and F. Larachi, "Mechanistic model for structured-packing-containing columns: irrigated pressure drop, liquid holdup, and packing fractional wetted area," *Industrial and Engineering Chemistry Research*, vol. 40, no. 23, pp. 5140–5146, 2001.

[25] E. Brunazzi, G. Nardini, A. Paglianti, and L. Petarca, "Interfacial area of Mellapak packing: absorption of 1,1,1-trichloroethane by Genosorb 300," *Chemical Engineering & Technology*, vol. 18, no. 4, pp. 248–255, 1995.

[26] M. Henriques De Brito, U. Von Stockar, A. Menendez Bangerter, P. Bomio, and M. Laso, "Effective mass-transfer area in a pilot plant column equipped with structured packings and with ceramic rings," *Industrial & Engineering Chemistry Research*, vol. 33, no. 3, pp. 647–656, 1994.

[27] R. E. Tsai, A. F. Seibert, R. B. Eldridge, and G. T. Rochelle, "Influence of viscosity and surface tension on the effective mass transfer area of structured packing," *Energy Procedia*, vol. 1, pp. 1197–1204, 2009.

[28] S. Aferka, A. Viva, E. Brunazzi, P. Marchot, M. Crine, and D. Toye, "Tomographic measurement of liquid hold up and effective interfacial area distributions in a column packed with high performance structured packings," *Chemical Engineering Science*, vol. 66, no. 14, pp. 3413–3422, 2011.

[29] G. Q. Wang, X. G. Yuan, and K. T. Yu, "A method for calculating effective interfacial area of structured packed distillation columns under elevated pressures," *Chemical Engineering and Processing*, vol. 45, no. 8, pp. 691–697, 2006.

[30] J. R. Fair, A. F. Seibert, M. Behrens, P. P. Saraber, and Z. Olujic, "Structured packing performance—experimental evaluation of two predictive models," *Industrial and Engineering Chemistry Research*, vol. 39, no. 6, pp. 1788–1796, 2000.